Numerical study on material removal of a convex pattern surface interacting with non-spherical particles

Yan, Yunpeng; Pargalgauskas, Skirmantas; Helmons, Rudy; Schott, Dingena

DOI
10.1016/j.powtec.2023.119226

Publication date
2024

Document Version
Final published version

Published in
Powder Technology

Powder Technology 436 (2024) 119226

Contents lists available at ScienceDirect

Powder Technology

journal homepage: www.journals.elsevier.com/powder-technology

Numerical study on material removal of a convex pattern surface interacting with non-spherical particles

Yunpeng Yan [a,c,*], Skirmantas Pargalgauskas [a], Rudy Helmons [a,b], Dingena Schott [a,*]

[a] Department of Maritime and Transport Technology, Delft University of Technology, 2628 CD Delft, the Netherlands
[b] Department of Mineral Processing and HSE, Norwegian University of Science and Technology, 7031 Trondheim, Norway
[c] Key Laboratory for Bionics Engineering of Education Ministry, Jilin University, Changchun 130022, China

HIGHLIGHTS

- The convex pattern sample interacting with non-spherical particles displays the minimum wear.
- Wear volume of a plain sample is independent of particle shapes.
- The deformation of the convex pattern weakens the effectiveness of wear reduction.
- The sliding distances of individual non-spherical particles on the convex pattern sample are significantly reduced.

GRAPHICAL ABSTRACT

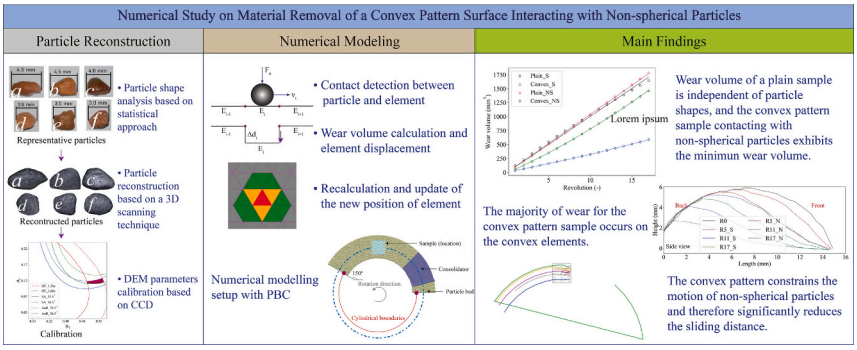

ARTICLE INFO

Keywords:
Particle shape
Wear reduction
Wear deformation
Convex pattern surface
DEM

ABSTRACT

A convex pattern surface is proposed and optimized to mitigate the sliding wear of bulk handling equipment caused by interaction with bulk solids. This work investigates the effectiveness of the convex pattern surface on wear reduction during interactions with non-spherical particles. Multiple representative particles, obtained through a sampling method, are reconstructed using a photogrammetry technique. Two contact parameters between particles are calibrated through shear box and drawdown tests to ensure flow behavior similar to the real material. The numerical results indicate that the convex pattern surface can effectively reduce wear compared to a plain sample when involving both spherical and non-spherical particles. For a plain sample, the wear volume remains independent of particle shapes and increases linearly with numerical revolutions. For the convex pattern surface, the wear volume demonstrates a quadratic relationship with the test revolutions as the deformation of convex elements weakens the effectiveness of the sample on wear reduction. The particle flow behavior analysis reveals that the convex pattern surface experiences the lowest wear volume when in contact with non-spherical particles. This can be attributed to the non-spherical particles sliding shorter distances and rotating with higher angular velocities on the convex pattern surface.

* Corresponding authors at: Department of Maritime and Transport Technology, Delft University of Technology, 2628 CD Delft, the Netherlands.
E-mail addresses: Y.Yan@tudelft.nl (Y. Yan), D.L.Schott@tudelft.nl (D. Schott).

https://doi.org/10.1016/j.powtec.2023.119226
Received 31 July 2023; Received in revised form 25 November 2023; Accepted 28 November 2023
Available online 2 December 2023

1. Introduction

Bulk solids handling plays a significant role in a range of industries, such as the mining, agricultural, chemical, and pharmaceutical industries [1]. Within the mining industry, the handling of bulk solids, such as iron ore, results in wear on the surfaces of bulking handling equipment. Studies show that approximately 82% of the energy loss is attributed to the bulk material sliding along the bottom of the chute, while 9% of the loss is due to the material sliding against the side walls [2]. Sliding wear can be defined as the relative movement occurring between two solid surfaces in contact while under a load [3]. Wear leads to surface deformation and hastens equipment damage, ultimately shortening its operational lifespan.

To reduce wear at micro [4,5] and macro [6] scales, a surface equipped with configurations (e.g. circular, triangular, and elliptical) is applied to the multiple fields mentioned above. For the elliptical texture, it has been used to reduce the wear of plows [7], drills [8], lubricated contacts [9], etc. In an effort to mitigate sliding wear on bulk solids handling equipment, an innovative convex pattern surface, inspired by a bionic design approach [10], is proposed [11] and further optimized [12] utilizing the discrete element method (DEM) [13].

Regarding wear evaluation, DEM proves to be a valuable approach in predicting equipment wear resulting from bulk material interactions. On one hand, DEM models wear without considering geometrical deformation, making it widely applicable in investigating the linear wear and distribution within various systems, such as ball mills [14–16], tumbling mills [17–19], mining hoppers [20], agricultural tines [21], and soil rapper tins [22], etc. On the other hand, researchers express keen interest in surface deformation caused by bulk material contact, such as, estimations of adhesion, abrasion, and impact wear in dry ball mills [23], wear prediction for ball mill liners in the cement industry [24], modeling scratch tests to study abrasive material loss caused by soil tillage [25], and comparing wear profiles of screw liners [26]. To incorporate the deformation of convex pattern surfaces due to bulk material contact, DEM combined with geometry deformation techniques, is employed and validated by conducting laboratory experiments [27]. However, for computational efficiency, spherical particles are commonly employed to represent real particles, which may not accurately reproduce the flow behavior of actual materials [18].

Multiple models have been proposed to reconstruct non-spherical particles [28], such as the super-quadric model [29–31], polyhedron model [32–34], and multi-sphere model [35]. Sphere-based modeling as used in this study, stems from the idea of recreating a non-spherical shape by clumping multiple physically overlapped spheres (sub-particles). The particle morphology for reconstruction with spheres can be obtained through a 3D scanning technique named photogrammtery [36]. Combined with the sphere-based clumping model, this method can replicate the real particle shapes and simultaneously takes the computational efficiency into account by balancing the size and number of spherical particles.

As is concluded in our previous work that the convex pattern sample reduces wear for a short term experiment, it is significant to reveal whether the sample functions in a long term test numerically. The work aims to evaluate the effectiveness of the convex pattern sample on reducing sliding wear compared to a plain sample during the interaction with non-spherical particles. To accomplish this aim, the particle shape is reconstructed using a photogrammetry technique, and the corresponding parameters are calibrated for a numerical model. The mechanisms of the convex pattern sample on wear reduction are revealed by analyzing the numerical results including the wear volume, wear distribution, and the flow behavior of particles.

2. Methodology

The Discrete Element Method (DEM) is first introduced by Cundall and Strack [13] for the simulation of particle systems, enabling the monitoring of particle movements and interactions within their environment over time. The dynamics of discrete spheres in DEM are governed by the principles of Newton's second law of motion. Hertz–Mindlin no-slip contact model has been widely used and proven suitable for nonlinear elastic contact model [37]. This model is composed of two springs, two dampers, and a slider, as represented in Fig. 1, and it effectively characterizes the interactions among non-cohesive particles.

As illustrated in Fig. 2, the completion of surface deformation involves the integration of a geometrical deformation technique [38] within the EDEM software [39], complemented by the incorporation of the Archard wear model [40]. Notably, the highlighted section represents the process of wear volume calculation and subsequent mesh position updates for the geometry. For detailed explanation, we refer to our previous work [27].

3. Model preparation

The real particles of river gravel are reconstructed, and the corresponding parameters are calibrated to capture the flow behavior of particles displayed in laboratory experiments.

3.1. Particle shape reconstruction and calibration

The river gravel with d_{50} of 2.65 mm is used as a wear medium, which is classified as dry, non-cohesive, and free-flowing material. For detailed properties of this material, we refer to our previous work [12]. To reconstruct the particles for numerical modeling, three steps are applied.

3.1.1. Particle shape analysis

A multistage sampling approach is utilized to calculate the proportional distribution of particle shapes with a desired level of precision. Shown in Fig. 3, the overall material volume of 1400 ml is divided into 14 sections. From these sections, three samples are randomly selected for the next stage. Each of the three chosen samples is further divided into approximately equal subsections, resulting in 16 samples. Finally, two samples are randomly selected from each of the three samples for final analysis, with the total number of 368 particles.

The aforementioned material samples are evaluated following a comparable procedure outlined in reference [41]. By evaluating the particles based on four aspects, including aspect ratio, flatness, roundness, and the count of flat facet, the total 368 particles are classified into six distinct shape classes (designated as A to F), with the shape variants named according to their most visually distinctive property. Based on the classification criteria mentioned above, the shape of individual particles within all six material samples is determined, and the particle shape distribution is obtained.

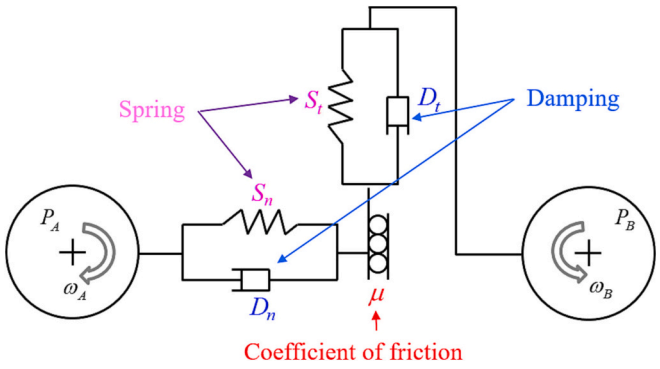

Fig. 1. Illustration of contact between two particles [27].

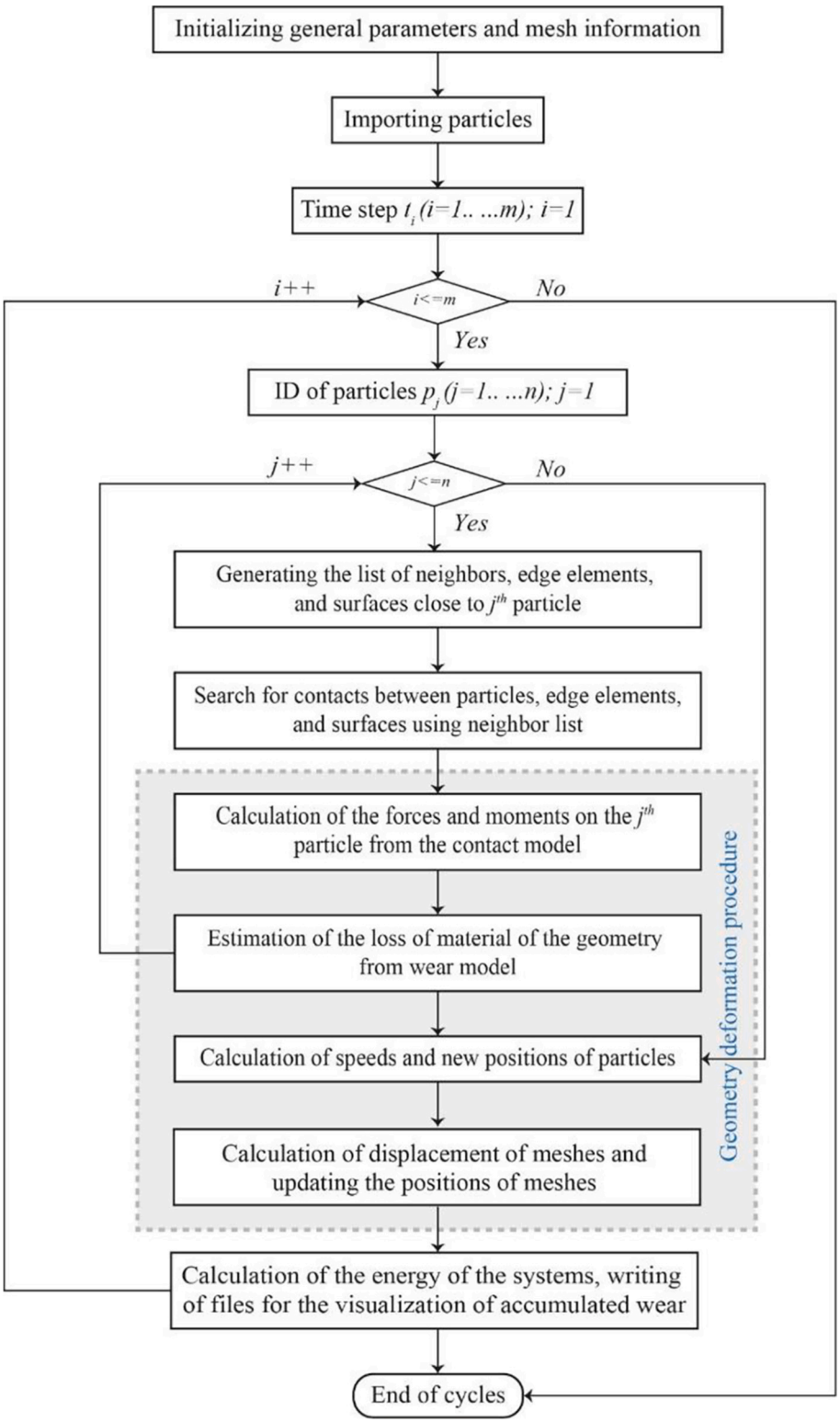

Fig. 2. Flowchart for calculating wear volume and updating deformation [27].

3.1.2. Particle shape reconstruction

As material is sampled and classified into 6 kind of shapes, a single particle of a relatively greater size is chosen to represent the characteristics of particles in the corresponding class illustrated in Fig. 4.

For the reconstruction of particles, 40–50 pictures around each particle are taken by adjusting the location of a camera under a controlled environment, such as lighting arrangement. A photogrammetry technique [36], capable of handling images with substantial overlap, is deployed to obtain a particle profile. Six mesh files are generated corresponding to the representative particles chosen for each shape class.

Spherical particles are used to fill the generated mesh files to reconstruct angular particles. The size and number of spherical particles for the clumping approach are manually controlled to be around 1 mm

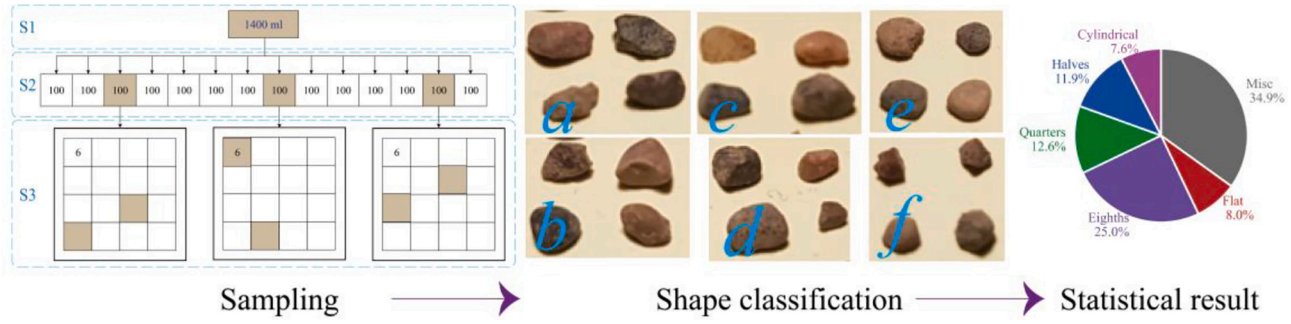

Fig. 3. Procedure of particle shape analysis.

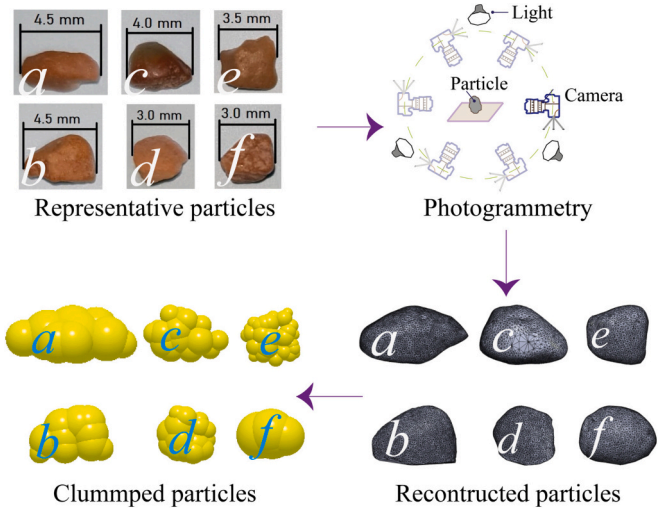

Fig. 4. Procedure of particle shape analysis.

and greater than 6 to balance modeling accuracy and computational efficiency. It should be noted that the clumped particles are rounded, so it ensures a comparable surface roughness for both the spherical and non-spherical particles.

3.1.3. DEM parameter calibration

The shear box and drawdown tests are carried out to characterize the relevant bulk properties (coefficients of static and rolling friction μ_s, μ_r) as depicted in Fig. 5. The corresponding parameters, including the physical characteristics of the river gravel, the material properties used in the tests, are listed in Table 1. For detailed test process, we refer to our previous work [12].

The calibration of DEM parameters, including the coefficients of static friction and rolling friction between particles, is performed using a surface response method called Central Composite Design (CCD) as depicted in Fig. 5. CCD is a partial factorial approach that is generally used to estimate effect curvature and for obtaining an optimal response. This method is suited for estimating small number of parameters as it possesses a moderate number of runs and predicts parameters with high accuracy. Once maximum and minimum values of each parameter are chosen, the parameter α is determined to be $\sqrt{2}$. Table 2 presents the coded and uncoded values of the two parameters.

Table 1
Parameters for numerical model.

Categories	Parameters	Values
River sand	Particle density (kg/m^3)	2460
	Poisson ratio ν (−)	0.24
	Shear modulus G (GPa)	0.07
Perspex	Density (kg/m^3)	1200
	Poisson ratio (−)	0.5
	Shear modulus G (GPa)	0.1
Steel	Density (kg/m^3)	7932
	Poisson ratio ν (−)	0.3
	Shear modulus G (GPa)	78
Particle-particle	Coefficient of restitution	0.45
	Coefficient of restitution (−)	0.4
Particle-perspex	Coefficient of static friction (−)	0.36
	Coefficient of rolling friction (−)	0.36
	Coefficient of restitution (−)	0.6
Particle-steel	Coefficient of static friction (−)	0.38
	Coefficient of rolling friction (−)	0.3

Table 2
Values of the two parameters.

Level	−α	−1	0	1	+α
μ_s	0.2	0.258	0.4	0.541	0.6
μ_r	0	0.035	0.12	0.205	0.24

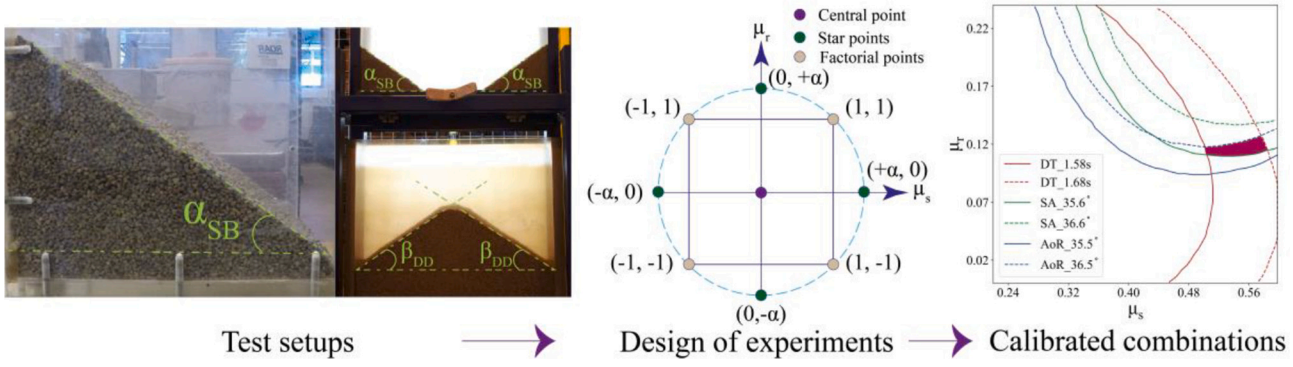

Fig. 5. Flowchart of particle reconstruction and parameter calibration.

Based on the design combination as illustrated in Fig. 5, the relationship between inputs (coefficients of static and rolling frictions) and outputs (discharge time, shear angle, angle of repose) of the shear box and drawdown test is presented in one plot where the shaded area indicates the possible combinations of the two coefficients. To avoid selecting the values at the boundaries, the static and rolling friction of coefficients are determined from the center of the shaded region, which are 0.548 and 0.116, respectively.

3.2. Simulation setup

The concept of a convex pattern surface depicted in Fig. 6, which was originally proposed in [42], is defined by five parameters [12]. To perform an in-depth analysis of wear distribution, the sample is divided into five columns and labeled with identifiers (e.g., Col_1 signifies column 1) in the bulk flow direction. Futhermore, the convex elements are individually labeled from the inside to the outside of the test setup.

The configuration of the DEM simulation is demonstrated in Fig. 7. To enhance computational efficiency, cylindrical boundaries covering 150 degrees are implemented, enabling particles exiting from one side to re-enter at corresponding locations at the opposite side. The particle size is scaled up by a factor of 3 based on previous findings which indicat that particle size has minimal impact on the sliding wear of the plain sample, while the convex pattern sample reduces wear with a scaling factor lower than 4 [43]. To ensure a uniform particle bed, a consolidator is employed. The test sample is positioned at a depth of 90 mm, inclined at an angle of 2 degrees. The particle bed rotates at a rate of 90 degrees per second, with 1.67 s to complete a 150-degree revolution. For further details on other parameters utilized in the numerical model, one can refer to the previous study [12].

4. Result analysis

4.1. Wear comparison

The numerical results are analyzed from two aspects: the comparison of wear volumes of samples corresponding to different particle shapes and the flow behavior of particles at the contact interface with the sample. It should be noted that the numerical results are based on the simulations after reaching a steady state. For detailed analysis, one can refer to the previous work [27].

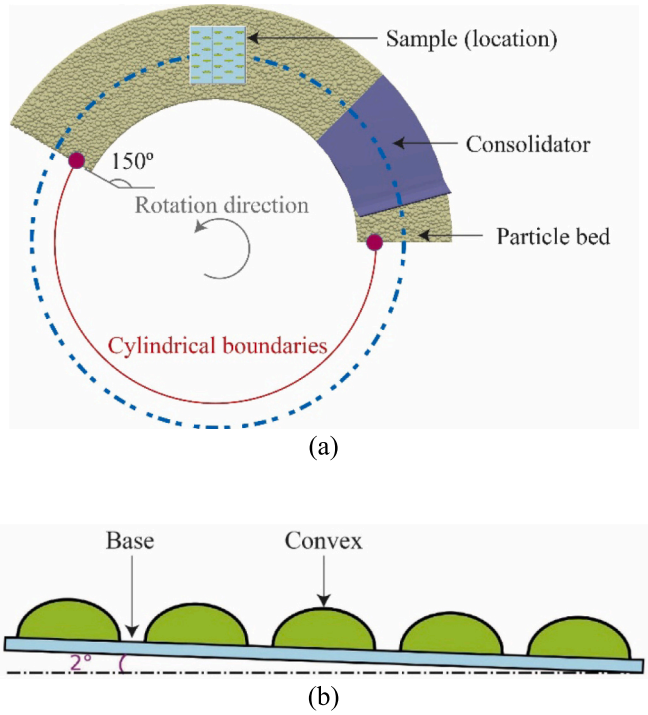

Fig. 7. Simulation setup (a) particle bed settings, (b) inclination angle of sample [27].

4.1.1. Wear volume

Fig. 8 compares the wear volume of the plain and convex pattern surfaces contacting with the corresponding spherical and non-spherical particles. Eqs. (1)–(4) shown below indicates the relationship between simulation revolution and wear volume for spherical and non-spherical particles contacting with a plain and a convex pattern surface, respectively. It should be noted that the simulation terminates due to the mesh distortion as explained in the previous work [27].

For a plain surface, wear volume is independent of particle shape and

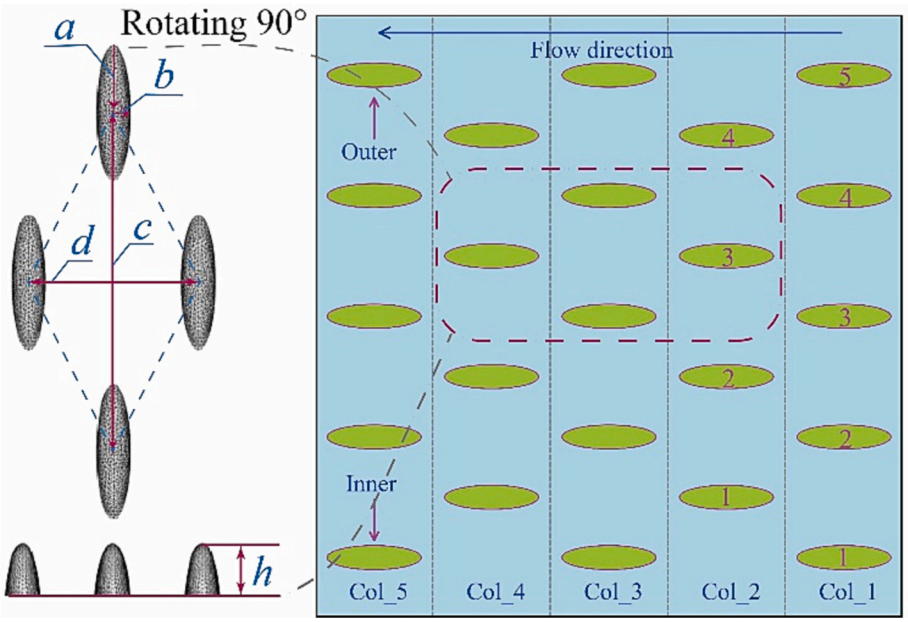

Fig. 6. Convex pattern sample (a = 8 mm, b = 2 mm, c = 40 mm, d = 20 mm, h = 6 mm) [27].

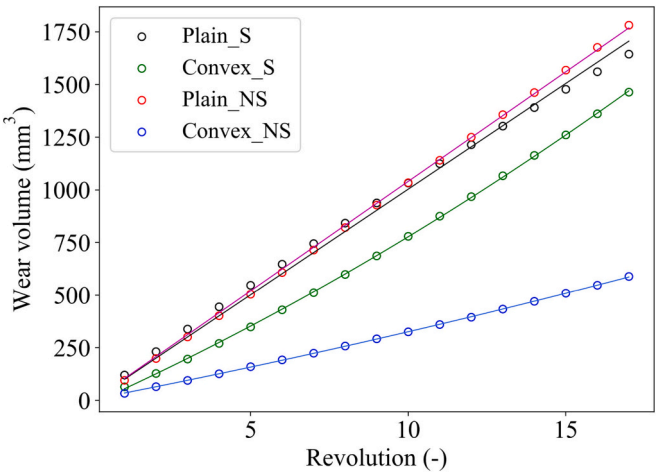

Fig. 8. Wear volume in relation to revolution (S and NS indicate spherical and non-spherical particles.)

has a linear relationship with the numerical revolution as denoted in Eq. (1) and Eq. (2). For the convex pattern surface, the wear volume is lower than that of a plain surface and has a quadratic relationship with the revolution as denoted in Eq. (3) and Eq. (4). This indicates that the wear rate of the convex pattern surface increases as a result of the deformation of the convex elements, which is consistent with the previous work [27]. Moreover, the wear volume of the convex pattern surface is dependent on particle shape. Fig. 8 indicates that the convex pattern surface due to the contact with non-spherical particles results in significantly less wear compared to that corresponding to the spherical particles.

$$y = 100.3x, R^2 = 0.9941 \tag{1}$$

$$y = 104.0x, R^2 = 0.9996 \tag{2}$$

$$y = 67.4x + 1.2x^2, R^2 = 0.9999 \tag{3}$$

$$y = 28.9x + 0.3x^2, R^2 = 0.9999 \tag{4}$$

To compare the wear volume of individual convex elements labeled in Fig. 6, the ratio of wear volumes of convex elements corresponding to non-spherical and spherical particles is applied as depicted in Fig. 9. As the number of convex elements in one column is distributed as either 5 or 3, to make it distinguishable, the columns with 5 elements are labeled as C135, and the first individual one from the inner side (indicated in Fig. 6) corresponding to the test is numbered 1. Similarly, each of the element can be termed with a specific label. Fig. 9 demonstrates that the non-spherical particles induce less wear compared to spherical particles for each individual convex element. Column 5 indicates the highest proportion of wear volume with a ratio from 52% to 84%, while the other four columns show a much lower proportion of wear volume less than 55%. For individual elements in each column, the elements at the ends of a column encounter more wear compared to the rest. How this is relates to the flow behavior of particles will be discussed in detail in 4.2.

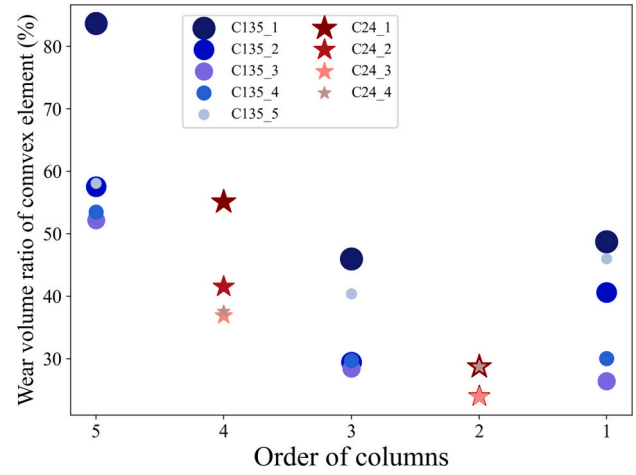

Fig. 9. Ratio of wear volume of convex elements with spherical particles to those with non-spherical particles.

4.1.2. *Wear distribution and deformation reconstruction*

Fig. 10 displays the wear distribution of plain and convex pattern samples in contact with spherical and non-spherical particles after 17 revolutions, respectively. Due to the contact with spherical particles, the wear depth for the plain sample depicted in Fig. 10 (a) is almost evenly distributed over the plain sample. For the convex pattern sample shown in Fig. 10 (b), wear paths are formed among the convex elements due to the flow behavior of particles. Futhermore, the majority of wear is transferred to the convex pattern, thus protecting the base. Due to the contact with non-spherical particles, the plain sample shown in Fig. 10 (c) displays a similar wear distribution as for spherical particles. For the convex pattern sample, similarly, the majority of wear is distributed over the convex elements, while the base encounters much less wear compared to spherical particles. Comparing the magnitude of the wear depth for both plain and convex pattern samples, it indicates that the spherical particle induces more wear than non-spherical particles, which is consistent with the presented wear volumes in Fig. 9.

Furthermore, Fig. 11 compares the deformation process of three convex elements in column 1, since this column has the severest deformation as shown in Fig. 10. For the three convex elements, the spherical particles induce severer deformation than non-spherical particles, which is consistent with the wear depth distribution shown in Fig. 10. For each convex element, from the side view, these three convex elements follow a similar deformation trend. The front part of the convex elements shows the severest deformation, since this part comes into direct contact with particles. From the front view, it indicates that the inner side of C11 and the outer side of C15 show greater deformation. This implies that the convex pattern barely affects the flow behavior of particles at the two sides [12]. Furthermore, C15 is subject to the greatest degree of deformation because the particles at the outer end of a circular wear tester slide longer distances.

To explicitly compare the wear depth of the convex elements, the middle section of the side view of C15 (Fig. 11 (C)) at the range between 7.5 mm to 8.5 mm is selected as a reference fragment. An average value of the points included in this range is considered the height of the element at a specific revolution. For spherical particles, the height of the element C15 drops significantly from 6.17 mm to 0.9 mm, resulting in an average wear depth of 0.31 mm per revolution. On the contrary, when contacting with non-spherical particles, the convex pattern sample indicates a moderate deterioration of convex element from 6.17 mm to 2.95 mm, leading to the average wear depth of 0.19 mm per revolution.

4.2. *Particle flow behavior*

Particle flow behavior is evaluated from macroscale and microscale aspects. The macroscale aspect investigates the flow behavior of bulk solids, consisting of the angular and transitional velocity of particles at the contact interface with a test sample. The microscale aspect compares the trajectories of individual particles with different shapes contacting with different samples.

4.2.1. *Flow behavior of bulk solids*

Fig. 12 compares the magnitude of the velocity of particles contacting with a sample. For both spherical and non-spherical particles, the particles contacting with a plain surface have higher velocity compared to those contacting with the convex pattern surface. It indicates that the

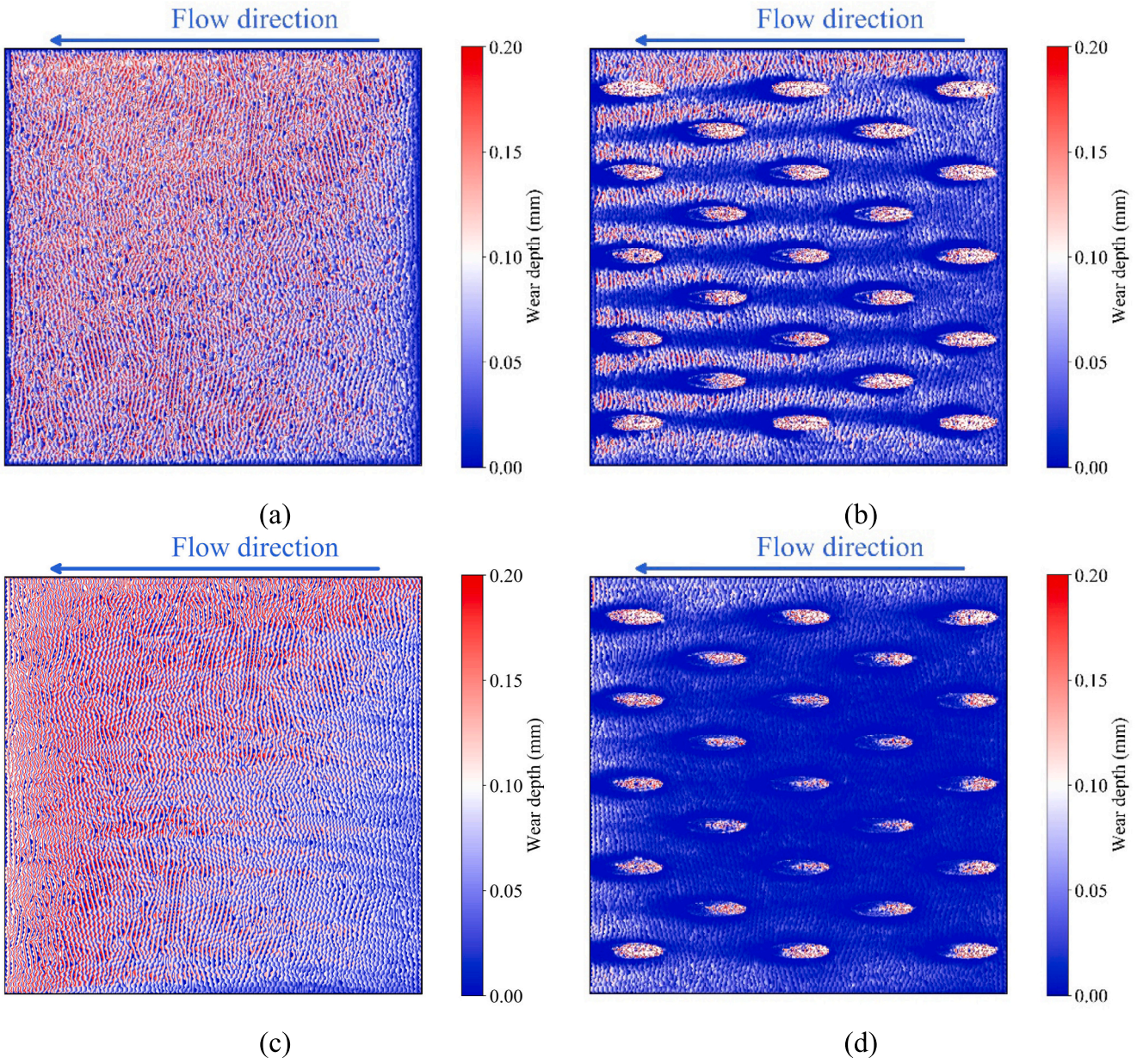

Fig. 10. Wear depth profile (a) plain sample due to spherical particles, (b) convex pattern sample due to spherical particles, (c) plain sample due to non-spherical particles, and (d) convex pattern sample due to non-spherical particles.

convex pattern slows down the motion of particles and therefore reduces the sliding distance over the convex pattern surface. For the plain sample, the non-spherical particles have the highest velocity and stay in a relatively small range from 477 ± 37 mm/s to 529 ± 19 mm/s, while the velocity of spherical particles decreases slowly from 499 ± 14 mm/s to 410 ± 20 mm/s. For the convex pattern sample, on the other hand, the spherical particles move faster than non-spherical particles, with ranges from 186 ± 28 mm/s to 282 ± 23 mm/s and from 85 ± 26 mm/s to 122 ± 24 mm/s, respectively. It means that the non-spherical particles slide the lowest distance on the convex pattern surface.

To compare the velocity distribution of particles on the samples, a mesh grid with 20 × 20 elements is deployed to capture the average velocity in each individual element. Each of the elements has a dimension of 5 mm × 5 mm × 6 mm (length×width×height). Fig. 13 displays the average velocity of particles in each element over 17 revolutions. For the plain sample shown in Fig. 13 (a) and (c), the particles at the outer side demonstrated in Fig. 6 flow faster than those at the inner side due to the effect of the rotation of the particle bed. Fig. 13 (c) shows that the non-spherical particles have higher velocity compared to the spherical particles shown in Fig. 13 (a). For the convex pattern surface, the spherical and non-spherical particles indicate a similar velocity distribution displayed in Fig. 13 (b) and Fig. 13 (d). The particles close to the center of the sample flow slower compared to those at the two sides, which indicates that the convex pattern hinderes he sliding of particles. This phenomenon is more obvious for non-spherical particles, so the motion of the non-spherical particles is significantly constrained by the convex pattern.

Similarly, the average angular velocity of particles is evaluated as shown in Fig. 14. On the contrary, for each type of particle, the convex pattern surface increases the angular velocity compared to a plain surface, which relies on the effect of the convex pattern on facilitating the rotation of particles as explained in the previous work [27]. For both the plain and convex pattern samples, it shows that non-spherical particles have higher angular velocity compared to spherical particles. This phenomenon can be explained by comparing the moment of inertia between spherical and non-spherical particles. For the spherical

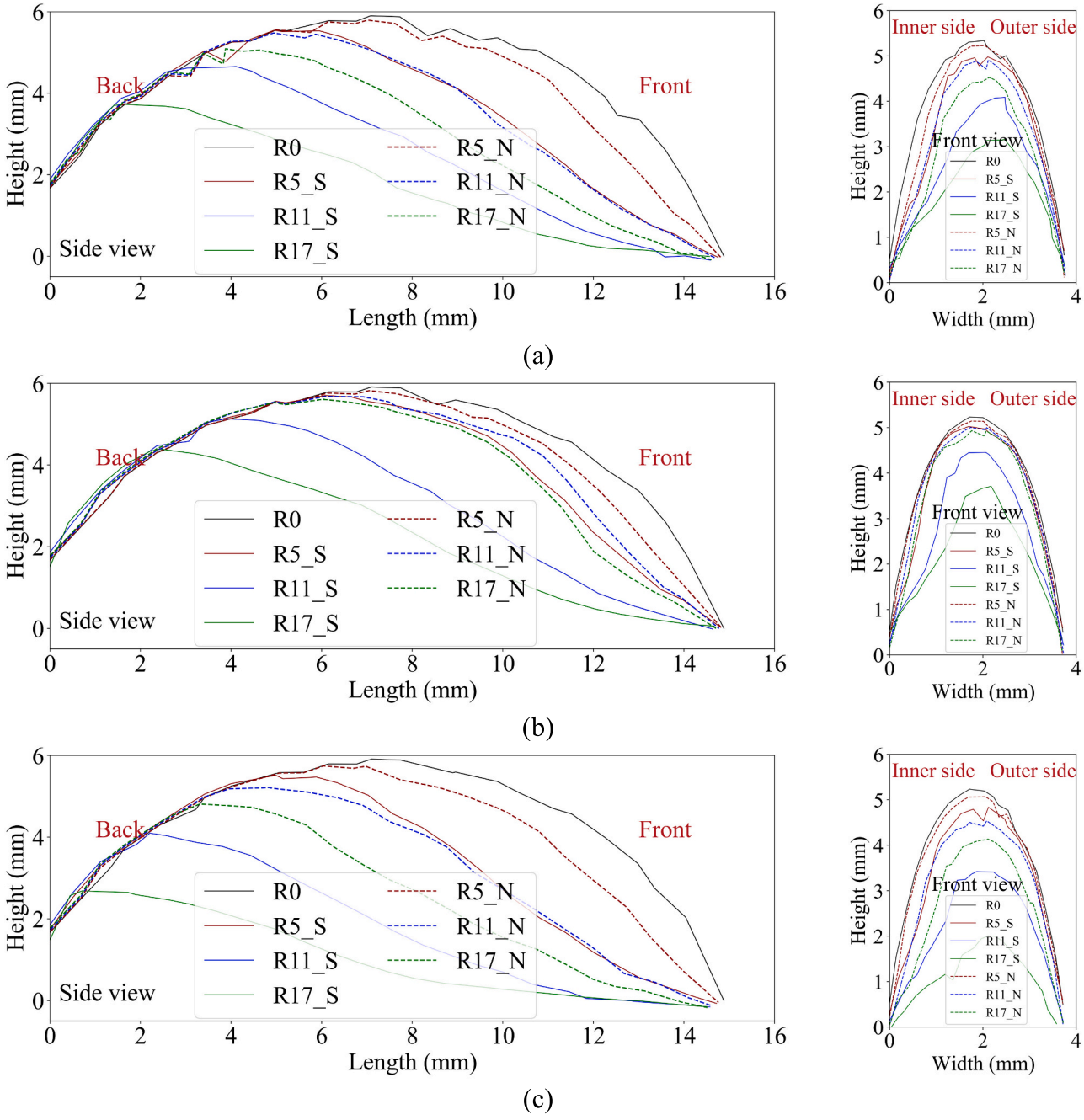

Fig. 11. Reconstruction of convex elements (a) C11, (b) C13, and (c) C15 (R, S, and N indicate revolution, spherical, and non-spherical, respectively.)

particles contacting with a sample, the average moment of inertia for an individual particle is 8.4×10^{-9} kg•m^2, while this is 4.9×10^{-9} kg•m^2 for non-spherical particles. This means a higher force needs to be applied to a spherical particle to induce a rotation equivalent to that of a non-spherical particle. Combining the effect of the convex pattern on improving the rotation of particles, the non-spherical particles demonstrate the highest angular velocity ranging from 458 ± 45 deg./s to 680 ± 50 deg./s.

Fig. 15 displays the distribution of angular velocity for both spherical and non-spherical particles contacting with the plain and convex pattern surfaces. It can be seen from Fig. 15 (a) and (c) that the particles at the outside of samples rotate faster than those at the inner side as illustrated in Fig. 7, which is consistent with the trend of particle velocity shown in Fig. 12. For the convex pattern surface, the particles close to the center of the sample display lower angular velocity, which is consistent with the distribution of particle velocity. Combined with the velocity distribution shown in Fig. 12, it implies that the plain sample barely affects the motion of particles. However, for the convex pattern sample, it alters the flow behavior of particles by simultaneously inhibiting the sliding velocity and facilitating the rolling velocity.

4.2.2. *Flow behavior of individual particles*

To understand the direct flow behavior of individual particles, the trajectories of multiple particles contacting with the samples in one revolution are reconstructed as illustrated in Fig. 16. When particles enter the surface of a sample, the positions of the selected particles are recorded until the end of a revolution. It should be noted that the particle bed rotates counterclockwise, and the particles are randomly selected. For the plain sample displayed in Fig. 16 (a) and (c), the spherical and non-spherical particles almost return to the starting

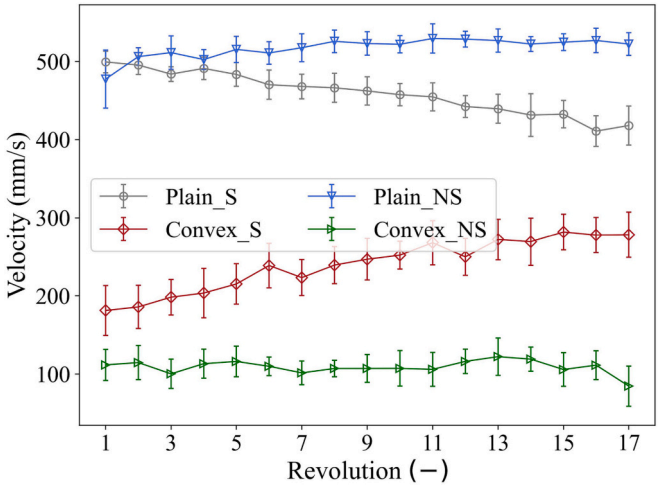

Fig. 12. Velocity of particles at bottom layer (Error bar indicates the standard deviation.)

points, which means that the plain sample has a negligible effect on altering the flow behavior of particles. For the convex pattern sample shown in Fig. 16 (b) and (d), the trajectories of spherical particles are slightly influenced by the contact with the convex elements, while the non-spherical particles (especially the particles in the middle of the sample) only form much shorter trajectories. This indicates that the convex pattern constrains the motion of non-spherical particles and

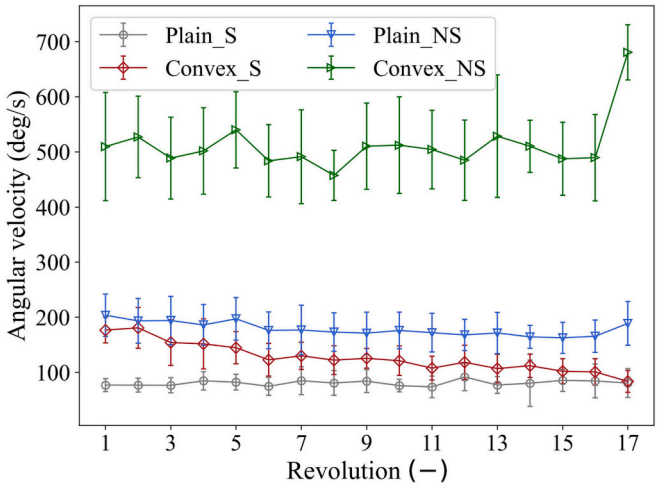

Fig. 14. Angular velocity of particles at bottom layer.

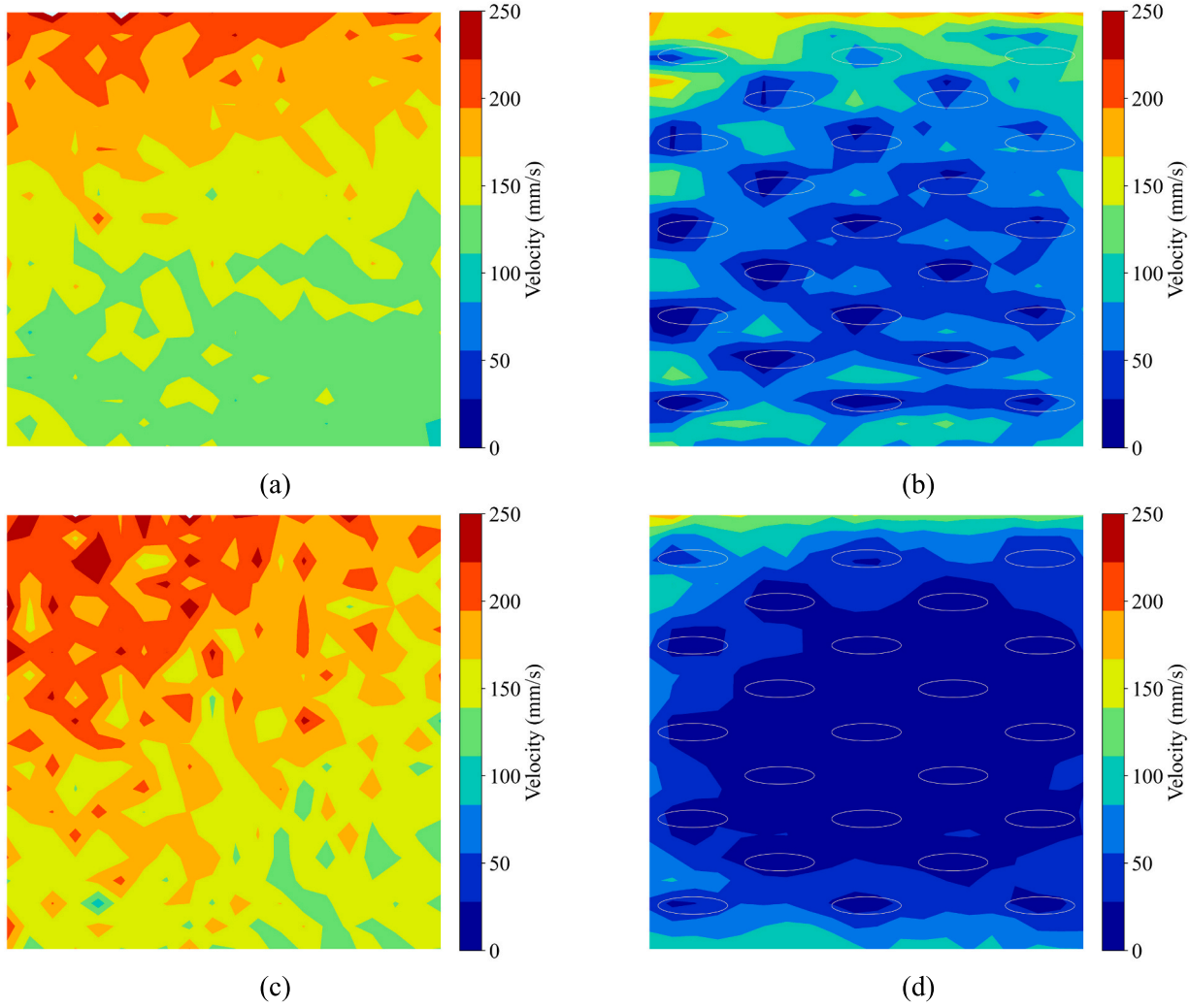

Fig. 13. Velocity profile of particles at bottom layer with (a) spherical particles on plain surface, (b) spherical particles on convex pattern surface, (c) non-spherical particles on plain sample, and (d) non-spherical particles on convex pattern surface.

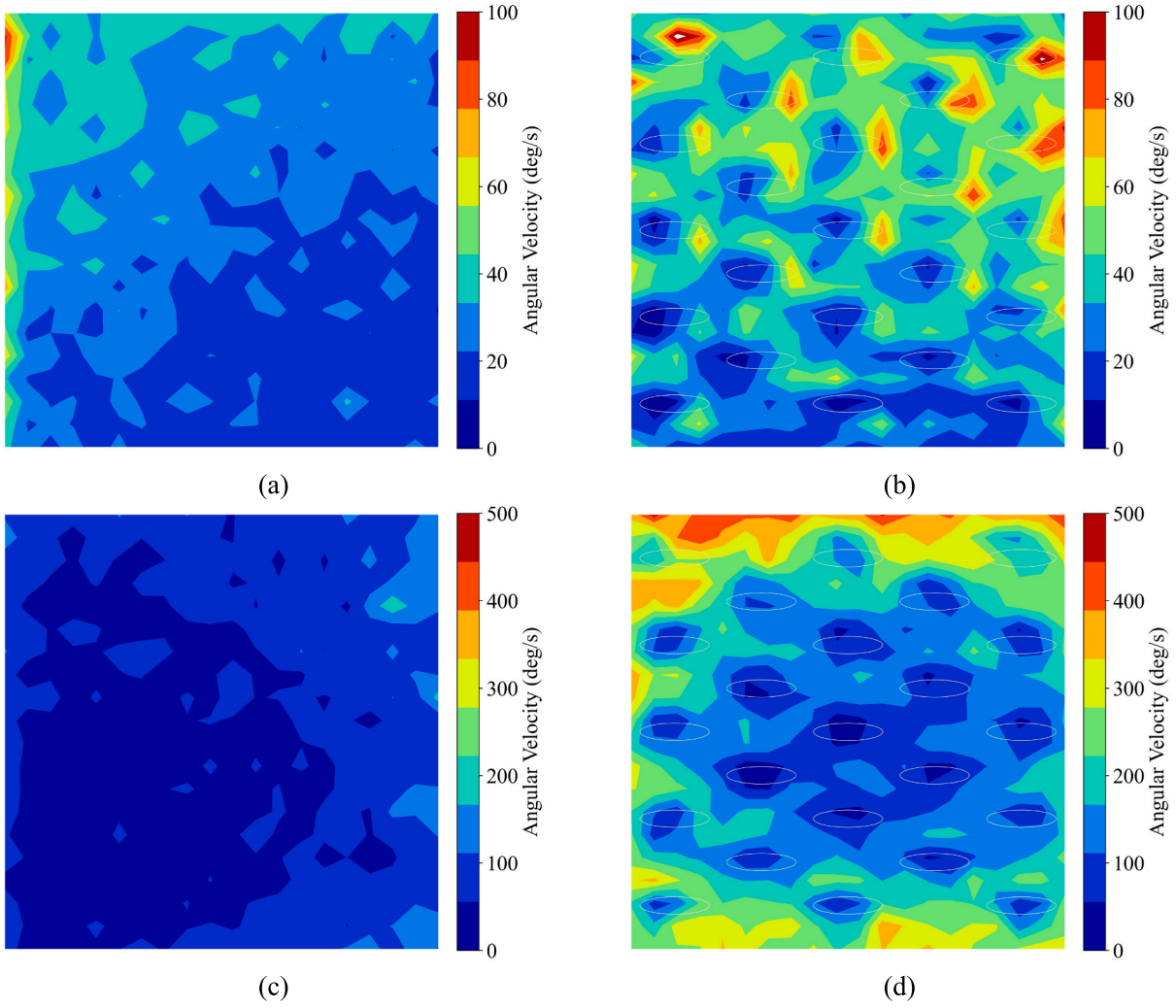

Fig. 15. Angular velocity profile of particles at bottom layer with (a) spherical particles on plain surface, (b) spherical particles on convex pattern surface, (c) non-spherical particles on a plain sample, and (d) non-spherical particles on the convex pattern surface.

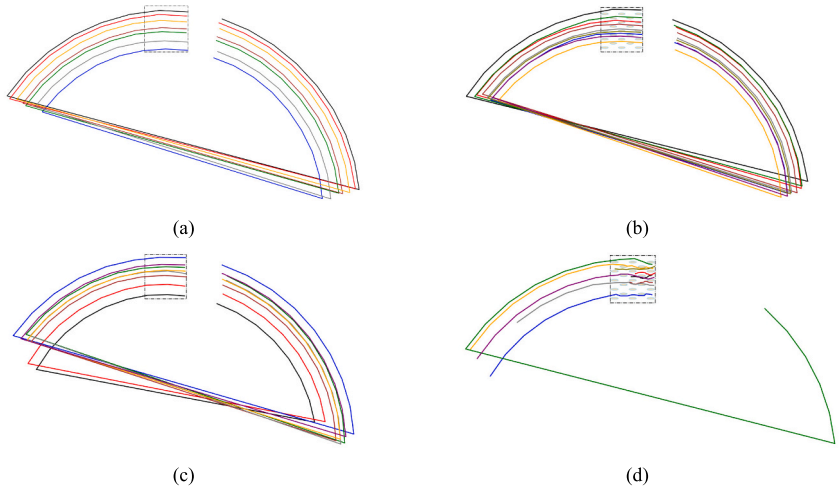

Fig. 16. Trajectories of particles in one revolution (a) spherical particles on plain surface, (b) spherical particles on convex pattern surface, (c) non-spherical particles on plain sample, and (d) non-spherical particles on the convex pattern surface.

therefore significantly reduces the sliding distance. This phenomenon enhances the explanation of the lowest wear volume of a convex pattern surface when contacting with non-spherical particles.

5. Conclusions

This study investigates the effects of particle shape on the deformation of a convex pattern sample caused by sliding wear. The work aims to reveal the effectiveness of the convex pattern sample in reducing sliding wear compared to a plain sample when referring to non-spherical particles.

The non-spherical particles reflecting the flow behavior of real materials are modelled by clumping multiple spherical particles. Using a multi-step sampling approach, representative particle shapes are identified, and their profiles are extracted through photogrammetry scanning. To model non-spherical particles, multiple spherical particles within a specific size range are clumped together, ensuring modeling precision and computational efficiency. The flow behavior of the bulk material is characterized by calibrating the coefficients of static and rolling friction using a central composite design method.

The numerical results indicate that the convex pattern surface reduces wear compared to a plain sample under contact with both spherical and non-spherical particles. For a plain sample, the wear volume is independent of particle shapes and has a linear relation with the numerical revolutions. For the convex pattern sample, on the other hand, the wear volume is closely related to particle shapes and increases quadratically with numerical revolutions, with minimum wear volume contacting with non-spherical particles.

For the wear distribution, most of the wear for the convex pattern sample concentrates on the convex elements and therefore the base of the sample is protected. The front part of the convex elements displays the severest deformation as this part directly contacts with particles.

The essential mechanism of the convex pattern sample on wear reduction relies on altering the flow behavior of particles. The contact behavior of particles at the bottom layer indicates that the convex pattern decelerates the transitional velocity of particles and facilitates rolling, which leads to a shorter sliding distance than on a plain sample. This phenomenon is more obvious when a convex pattern sample contacts with non-spherical particles.

Future work would focus on the reconstruction of particles with sharp corners to guarantee similar particle shape morphologies with those in practice. Considering the non-spherical particles reducing wear for the convex pattern surface by significantly exhibiting the flow of particles, priority should be given to addressing the resulting consequences, such as blockages or high energy consumption during bulk handling, rather than solely focusing on wear reduction.

CRediT authorship contribution statement

Yunpeng Yan: Conceptualization, Data curation, Formal analysis, Funding acquisition, Investigation, Methodology, Project administration, Resources, Software, Supervision, Validation, Visualization, Writing – original draft, Writing – review & editing. **Skirmantas Pargalgauskas:** Data curation, Formal analysis, Investigation, Methodology, Resources, Software, Visualization, Writing – original draft. **Rudy Helmons:** Conceptualization, Supervision, Writing – review & editing. **Dingena Schott:** Conceptualization, Project administration, Supervision, Writing – review & editing.

Declaration of Competing Interest

This paper has no conflict of interest.

Credit Statement.

Conceptualization, Yunpeng Yan; data curation, Yunpeng Yan, Skimantas Pargalgauskas; formal analysis, Yunpeng Yan, Skimantas Pargalgauskas; funding acquisition (CSC No. 201806170036), Yunpeng Yan; investigation, Yunpeng Yan, Skimantas Pargalgauskas; methodology, Yunpeng Yan, Skimantas Pargalgauskas; project administration, Rudy Helmons, Dingena Schott; resources, Skimantas Pargalgauskas, Yunpeng Yan; software, Skimantas Pargalgauskas, Yunpeng Yan; supervision, Rudy Helmons and Dingena Schott; visualization, Yunpeng Yan, Skimantas Pargalgauskas; writing—original draft, Yunpeng Yan; Writing—review & editing, Yunpeng Yan, Rudy Helmons, Dingena Schott. All authors have read and agreed to the published version of the manuscript.

Data availability

Data will be made available on request.

References

[1] D. Schulze, Powders and Bulk Solids: Behavior, Characterization, Storage and Flow 2008, 2003.

[2] A.W. Roberts, Chute performance and design for rapid flow conditions, Chem. Eng. Technol. 26 (2003) 163–170, https://doi.org/10.1002/ceat.200390024.

[3] I. Hutchings, P. Shipway, Sliding Wear, 2nd ed, Elsevier Ltd., 2017, https://doi.org/10.1016/b978-0-08-100910-9.00005-2.

[4] H.L. Costa, J. Schille, A. Rosenkranz, Tailored surface textures to increase friction—a review, Friction. 10 (2022) 1285–1304, https://doi.org/10.1007/s40544-021-0589-y.

[5] M. Marian, A. Almqvist, A. Rosenkranz, M. Fillon, Numerical micro-texture optimization for lubricated contacts—a critical discussion, Friction. (2022), https://doi.org/10.1007/s40544-022-0609-6.

[6] H. Yu, Z. Han, J. Zhang, S. Zhang, Bionic design of tools in cutting: reducing adhesion, abrasion or friction, Wear. 482–483 (2021) 203955, https://doi.org/10.1016/j.wear.2021.203955.

[7] B. Chirende, J. Li, L. Wen, T.E. Simalenga, Effects of bionic non-smooth surface on reducing soil resistance to disc ploughing, Sci. China Technol. Sci. 53 (2010) 2960–2965, https://doi.org/10.1007/s11431-010-4128-8.

[8] X.F. Yang, R. Xia, H.W. Zhou, L. Guo, L.J. Zhang, Bionic surface design of cemented carbide drill bit, Sci. China Technol. Sci. 59 (2016) 175–182, https://doi.org/10.1007/s11431-015-5942-9.

[9] D. Gropper, L. Wang, T.J. Harvey, Hydrodynamic lubrication of textured surfaces: a review of modeling techniques and key findings, Tribol. Int. 94 (2016) 509–529, https://doi.org/10.1016/j.triboint.2015.10.009.

[10] J.F.V. Vincent, O.A. Bogatyreva, N.R. Bogatyrev, A. Bowyer, A.K. Pahl, Biomimetics: its practice and theory, J. R. Soc. Interface 3 (2006) 471–482, https://doi.org/10.1098/rsif.2006.0127.

[11] G. Chen, Surface Wear Reduction of Bulk Solids Handling Equipment Using Bionic Design, Delft University of Technology, 2017.

[12] Y. Yan, R. Helmons, C. Wheeler, D. Schott, Optimization of a convex pattern surface for sliding wear reduction based on a definitive screening design and discrete element method, Powder Technol. 394 (2021) 1094–1110, https://doi.org/10.1016/j.powtec.2021.09.041.

[13] P.A. Cundall, O.D.L. Strack, A discrete numerical model for granular assemblies, Geotechnique. 29 (1979) 47–65, https://doi.org/10.1680/GEOT.1979.29.1.47.

[14] P.W. Cleary, Predicting charge motion, power draw, segregation and wear in ball mills using discrete element methods, Miner. Eng. 11 (1998) 1061–1080, https://doi.org/10.1016/s0892-6875(98)00093-4.

[15] P.W. Cleary, P. Owen, Development of models relating charge shape and power draw to SAG mill operating parameters and their use in devising mill operating strategies to account for liner wear, Miner. Eng. 117 (2018) 42–62, https://doi.org/10.1016/j.mineng.2017.12.007.

[16] P.W. Cleary, M. Sinnott, R. Morrison, Analysis of stirred mill performance using DEM simulation: part 2 - coherent flow structures, liner stress and wear, mixing and transport, Miner. Eng. 19 (2006) 1551–1572, https://doi.org/10.1016/j.mineng.2006.08.013.

[17] L. Xu, S. Bao, Y. Zhao, Multi-level DEM study on liner wear in tumbling mills for an engineering level approach, Powder Technol. 364 (2020) 332–342, https://doi.org/10.1016/j.powtec.2020.02.004.

[18] L. Xu, K. Luo, Y. Zhao, J. Fan, K. Cen, Influence of particle shape on liner wear in tumbling mills: a DEM study, Powder Technol. 350 (2019) 26–35, https://doi.org/10.1016/j.powtec.2019.03.033.

[19] L. Xu, K. Luo, Y. Zhao, Numerical prediction of wear in SAG mills based on DEM simulations, Powder Technol. 329 (2018) 353–363, https://doi.org/10.1016/j.powtec.2018.02.004.

[20] E. Rojas, V. Vergara, R. Soto, Case study: discrete element modeling of wear in mining hoppers, Wear. 430–431 (2019) 120–125, https://doi.org/10.1016/j.wear.2019.04.020.

[21] Á. Kalácska, P. De Baets, D. Fauconnier, F. Schramm, L. Frerichs, J. Sukumaran, Abrasive wear behaviour of 27MnB5 steel used in agricultural tines, Wear. 442–443 (2020), https://doi.org/10.1016/j.wear.2019.203107.

[22] E. Katinas, R. Chotěborský, M. Linda, V. Jankauskas, Wear modelling of soil ripper tine in sand and sandy clay by discrete element method, Biosyst. Eng. 188 (2019) 305–319, https://doi.org/10.1016/j.biosystemseng.2019.10.022.

[23] J.T. Kalala, M.H. Moys, Discrete element method modelling of liner wear in dry ball milling, J. South. Afr. Inst. Min. Metall. 104 (2004) 597–602.
[24] D. Boemer, J.P. Ponthot, A generic wear prediction procedure based on the discrete element method for ball mill liners in the cement industry, Miner. Eng. 109 (2017) 55–79, https://doi.org/10.1016/j.mineng.2017.02.014.
[25] F. Schramm, V. Kalácska, J. Pfeiffer, P. De Sukumaran, L. Baets, Frerichs, modelling of abrasive material loss at soil tillage via scratch test with the discrete element method, J. Terramech. 91 (2020) 275–283, https://doi.org/10.1016/j.jterra.2020.08.002.
[26] P.M. Esteves, D.B. Mazzinghy, R. Galéry, L.C.R. Machado, Industrial vertical stirred mills screw liner wear profile compared to discrete element method simulations, Minerals. 11 (2021) 1–20, https://doi.org/10.3390/min11040397.
[27] Y. Yan, R. Helmons, M. Carr, C. Wheeler, D. Schott, Modelling of material removal due to sliding wear caused by bulk material, Powder Technol. 415 (2023) 118109, https://doi.org/10.1016/j.powtec.2022.118109.
[28] W. Zhong, A. Yu, X. Liu, Z. Tong, H. Zhang, DEM/CFD-DEM modelling of non-spherical particulate systems: theoretical developments and applications, Powder Technol. 302 (2016) 108–152, https://doi.org/10.1016/j.powtec.2016.07.010.
[29] Y. You, Y. Zhao, Discrete element modelling of ellipsoidal particles using super-ellipsoids and multi-spheres: a comparative study, Powder Technol. 331 (2018) 179–191, https://doi.org/10.1016/j.powtec.2018.03.017.
[30] P.W. Cleary, J.E. Hilton, M.D. Sinnott, Modelling of industrial particle and multiphase flows, Powder Technol. 314 (2017) 232–252, https://doi.org/10.1016/j.powtec.2016.10.072.
[31] P.W. Cleary, R.D. Morrison, Comminution mechanisms, particle shape evolution and collision energy partitioning in tumbling mills, Miner. Eng. 86 (2016) 75–95, https://doi.org/10.1016/j.mineng.2015.12.006.
[32] A. Wachs, L. Girolami, G. Vinay, G. Ferrer, Grains3D, a flexible DEM approach for particles of arbitrary convex shape - Part I: numerical model and validations, Powder Technol. 224 (2012) 374–389, https://doi.org/10.1016/j.powtec.2012.03.023.
[33] A.D. Rakotonirina, A. Wachs, Grains3D, a flexible DEM approach for particles of arbitrary convex shape - Part II: parallel implementation and scalable performance, Powder Technol. 324 (2018) 18–35, https://doi.org/10.1016/j.powtec.2017.10.033.
[34] A.D. Rakotonirina, J.Y. Delenne, F. Radjai, A. Wachs, Grains3D, a flexible DEM approach for particles of arbitrary convex shape—Part III: extension to non-convex particles modelled as glued convex particles, Comput. Part. Mech. 6 (2019) 55–84, https://doi.org/10.1007/s40571-018-0198-3.
[35] X. Wang, J. Yu, F. Lv, Y. Wang, H. Fu, A multi-sphere based modelling method for maize grain assemblies, Adv. Powder Technol. 28 (2017) 584–595, https://doi.org/10.1016/j.apt.2016.10.027.
[36] A. Paixão, R. Resende, E. Fortunato, Photogrammetry for digital reconstruction of railway ballast particles – a cost-efficient method, Constr. Build. Mater. 191 (2018) 963–976, https://doi.org/10.1016/j.conbuildmat.2018.10.048.
[37] J. Jäger, Elastic contact of equal spheres under oblique forces, Arch. Appl. Mech. 63 (1993) 402–412, https://doi.org/10.1007/BF00805740.
[38] F. Perazzo, R. Löhner, F. Labbe, F. Knop, P. Mascaró, Numerical modeling of the pattern and wear rate on a structural steel plate using DEM, Miner. Eng. 137 (2019) 290–302, https://doi.org/10.1016/j.mineng.2019.04.012.
[39] D.E.M. Solutions, EDEM 2.3 user guide, Edinburgh, Scotland, UK, 2010.
[40] J.F. Archard, Contact and rubbing of flat surfaces, J. Appl. Phys. 24 (1953) 981–988, https://doi.org/10.1063/1.1721448.
[41] C. Coetzee, Calibration of the discrete element method: strategies for spherical and non-spherical particles, Powder Technol. 364 (2020) 851–878, https://doi.org/10.1016/j.powtec.2020.01.076.
[42] G. Chen, D.L. Schott, G. Lodewijks, Bionic design methodology for wear reduction of bulk solids handling equipment, Part. Sci. Technol. 35 (2017) 525–532, https://doi.org/10.1080/02726351.2016.1144666.
[43] Y. Yan, R. Helmons, D. Schott, The influence of particle size on the sliding wear of a convex pattern surface, Minerals. 12 (2) (2021), https://doi.org/10.3390/min12020139.